NUMERICAL BEAM DYNAMICS STUDIES REGARDING CBETA CORNELL-BNL ERL

F. Méot, S. Brooks, D. Trbojevic, N. Tsoupas, BNL, Upton, Long Island, New York
S. Tygier, UMAN, Manchester*

Abstract

The Cornell-BNL Electron Test Accelerator CBETA is based on a 36 MeV super-conducting linac and on a single 4-pass up/4-pass down linear FFAG return loop, for beam acceleration from 6 to 150 MeV and energy recovery. Numerical beam dynamics simulations have accompanied and eventually validated the quadrupole-doublet FFAG cell technology and parameters, and following that the complete return loop, all along the ERL lattice design process. They are key to assessing and validating the ERL optics and beam behavior over the whole acceleration/ER cycle, and in preparing future machine operation. This paper presents various of these beam dynamics studies, including start-to-end simulations.

INTRODUCTION

The CBETA ERL return arcs and straight section are based on FFAG optics [1, 2]: a single return loop accepts all accelerated and decelerated passes (4 up and 4 down, 42, 78, 114 and 150 MeV). The optics is based on a quadrupole doublet which will be detailed in the following.

Once the parameters of that doublet are determined (an iterative optimization process), the 3D field maps of the two magnets are computed in OPERA, and then used for beam dynamics assessments based on stepwise ray-tracing and aimed at validating the magnet parameters that led to the field map of concern.

The present document is aimed at illustrating that stage of the CBETA lattice optical studies. This is done considering a particular quadrupole doublet, one amongst a series at a particular, intermediate, stage of that iterative process

PARAXIAL PROPERTIES OF CBETA CELL

The OPERA 3-D field maps of the magnets provide a realistic model of the CBETA cell (probably closest to real-life, until measured 3D field maps are available). Two methods have been used in the optimization process, namely, either using one field map for each quadrupole in the doublet cell, or using a single map of the complete cell. The first case is considered here. It requires managing the overlapping area of the extended field, between the two magnets (see Fig. 1), this is part of the numerical techniques and will not be discussed here.

* This work was performed with the support of NYSERDA (New York State Energy Research and Development Agency).

Accurate properties of FFAG cells can only be determined based on accurate field models [1] and that holds for orbits, focusing and higher order parameters including chromaticity, amplitude detuning, dynamical admittance, other feed down effects and other halo formation studies. OPERA 3-D field maps of the QF and BD provide that model. This requires stepwise integration of the equation of motion, which is the method retained in producing the beam dynamics results discussed here, using the ray-tracing code Zgoubi [6], and possibly its interface pyZgoubi [7] when it comes to end-to-end simulation of the complete CBETA ERL [8].

Due to the cell magnets being short, as was the case of the earlier, similar, EMMA FFAG cell [5], the field along the orbits does not feature any plateau (Fig. 1). As a consequence it has a rich content in derivatives (Fig. 2), as can be inferred from the scalar potential from which it derives, namely, $B_s = \partial V/\partial s$, $B_x = \partial V/\partial x$, $B_y = \partial V/\partial y$, with V a superposition of the multipole content

$$\begin{aligned} V_1(s,x,y) &= G_1(s)y - \frac{G_1^{(2)}(s)}{8}(x^2+y^2)y + \\ &\quad \frac{G_1^{(4)}(s)}{192}(x^2+y^2)^2y + \ldots \quad \text{(dipole)} \\ V_2(s,x,y) &= G_2(s)xy - \frac{G_2^{(2)}(s)}{12}(x^2+y^2)xy + \\ &\quad \frac{G_2^{(4)}(s)}{384}(x^2+y^2)^2xy + \ldots \quad \text{(quadrupole)} \\ V_3(s,x,y) &= etc. \end{aligned} \tag{1}$$

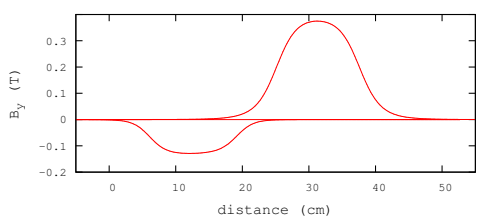

Figure 1: Typical field contributions along an orbit from the QF (left bump) and BD (right) magnets. The field in the numerical integration of particle motion is the sum of these two contributions.

In these expressions, s, x, y are respectively the longitudinal, transverse-horizontal and -vertical coordinates in the magnets with the latter two taken from the multipole axis, $G_{1,2}(s)$ is the longitudinal form factor and $G_{1,2}^{(n)} =$

[1] This is the lessons from the 1950s MURA studies which from the beginning leaned on computer based multi-turn stepwise ray-tracing [3], as well as from recent 150 MeV scaling FFAG ring R/D in Japan [4], and from the EMMA linear FFAG experiment [5] in which the cell happened to be similar to the present one.

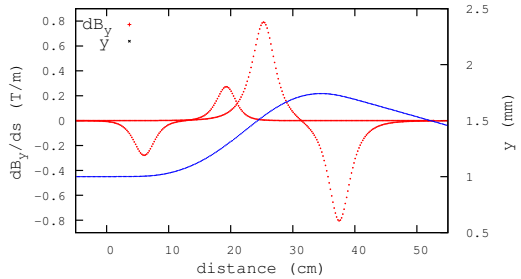

Figure 2: First order derivative dB_y/ds along QF and BD (red dotted curves) for trajectory with vertical coordinate represented by the blue curve (114 MeV). Field integrals do not cancel as the vertical coordinate changes across the magnets.

$d^nG_{1,2}/ds^n$. Note that non-zero vertical motion introduces horizontal orbit, and non-linear coupling.

An ideal cell without any random errors (neither field not alignment) is considered. Yet it does include systematic non-linearities, namely, (i) the multipole content intrinsic to the magnet geometry in the OPERA simulation, and (ii) the non-linearity content resulting from the longitudinal form factor as addressed above (Eqs. 1).

Periodic orbit excursions in the focusing quadrupole, QF, and in the defocusing quadrupole, BD, for all four energies, are displayed in Fig. 3. Fig. 4 shows the vertical magnetic field component along these orbits.

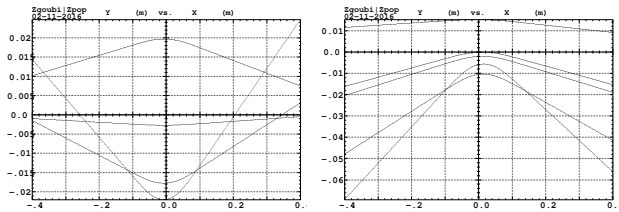

Figure 3: Typical periodic orbits in QF (left) and in BD (right) field maps, at 42, 78, 114 and 150 MeV.

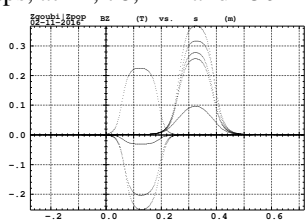

Figure 4: Typical vertical field component along orbits in QF (left) and BD (right), 42, 78, 114 and 150 MeV.

A scan of the paraxial tunes and chromaticities of the cell as of stepwise integration, thus including multipoles feed downs, is shown in Fig. 5. This establishes the optics working hypotheses, together with Table 1 which details paraxial tune values at the design energies.

LARGE AMPLITUDE

The OPERA 3-D field maps of the magnets give access to large amplitude properties of the particle motion and of the

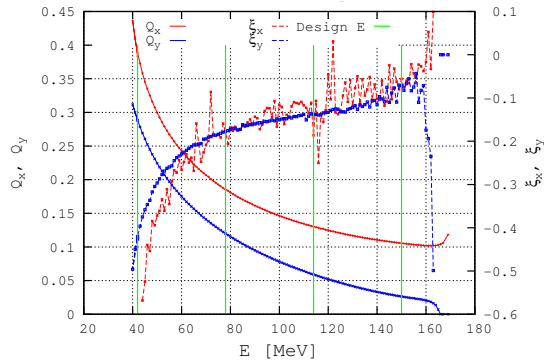

Figure 5: Typical energy dependence of tunes and chromaticities over [40,170]MeV, slightly beyond the {42,78,114,150} MeV set to check periodic stability margins. $\xi_{x,y}$ fluctuations are an artifact of field map usage.

beam line, such as dynamical admittance, amplitude detuning, non-linear coupling and beyond that, a tool to investigate such issues - out of the scope, here - as halo formation.

Large amplitude properties of the arc cell are summarized in Tab. 1 and in a series of figures, as follows.

Table 1: Tunes as a function of total energy, paraxial and, to give a taste of amplitude detuning, at maximum stable amplitudes either horizontal (case of extreme amplitude phase space motion as displayed in Fig. 8) or vertical (Fig. 9).

E [MeV]	42	78	114	150
Paraxial motion				
Q_x	0.3866	0.1840	0.1268	0.1004
Q_y	0.2978	0.1295	0.0676	0.0325
At maximum stable H amplitude				
Q_x	0.4001	0.1892	0.1303	0.1026
Q_y	0.2997	0.1216	0.0610	0.0247
At maximum stable V amplitude				
Q_x	0.3925	0.1805	0.1276	0.1790
Q_y	0.3010	0.1324	0.0763	0.0558

⋄ Dynamical admittances for a 1000-cell beam line (CBETA lattice counts ≈ 220 cells), as observed from the center of the long drift, are displayed Fig. 6, for the four design energies and two additional ones to assess viability margins beyond the useful range.

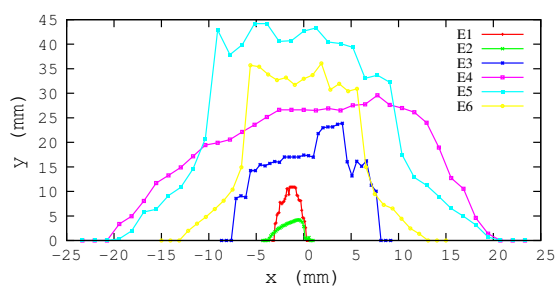

Figure 6: Dynamical admittance of a beam line made up of 1000 CBETA arc cells, at energies E1-6 = 40.5, 42, 78, 114, 150 and 160 MeV.

ISBN 978-3-95450-182-3

⋄ A scan of the admittance value over that extended energy interval 40.5-160 MeV, for a 200- or a 1000-cell beam line, is displayed in Fig. 7, which shows an increase from ≈7 mm at 42 MeV to ≈700 mm at 150 MeV. Note that 200 and 1000 cells produce similar results: any large amplitude particle loss is a matter of a reduced number of cell passes.

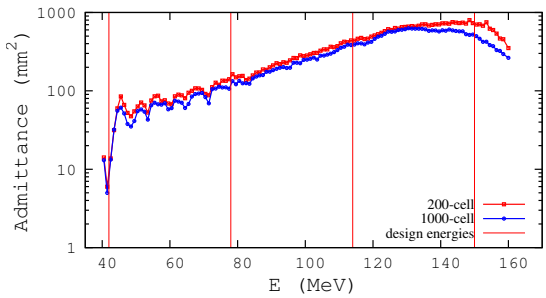

Figure 7: A scan in energy of arc-cell dynamical admittance value over 40.5-160 MeV, for 200-cell and 1000-cell beam lines, in an early version of the cell. Observation location is at center of 12 cm drift. Lattice parameters were tweaked to move the present dip in the 40 MeV region (due to the proximity of the $Qx + 2Q_y$ =integer resonance line, see Fig. 10) away from the low energy pass (see Ref. [2]).

⋄ Instances of maximum stable amplitude motion in phase space, *i.e.*, typical samples of the data that lead to the admittances in Figs. 6, 7, are displayed in Fig. 8 and Fig. 9 :

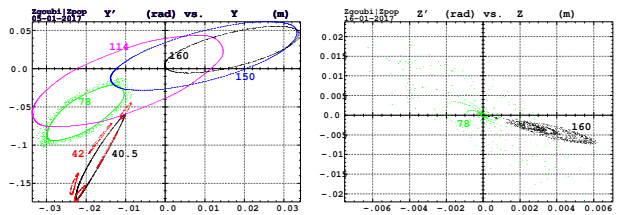

Figure 8: Left : 1000-cell maximum horizontal stable amplitude. Right : corresponding vertical phase-space - 78 MeV and 160 MeV undergo substantial growth, from quasi-zero initial invariant, the other 4 energies maintain their vertical invariant small.

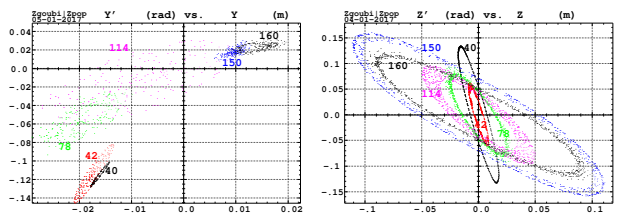

Figure 9: Right : 1000-cell maximum vertical stable amplitude. Left : corresponding horizontal phase-space, for quasi-zero initial horizontal invariant.

- In the horizontal phase space case, the initial vertical invariant is taken quasi-zero. The island portrait at 42 MeV stems from weak dodecapole non-linearities, while $Q_x = 2/5$ (Fig. 10). Coupling is significant at 78 MeV which spirals out to larger invariant and, outside nominal range, at 160 MeV which goes off-centered (Fig. 8-right).

- In the vertical phase space case, the initial horizontal invariant is taken quasi-zero, however, non-linear coupling causes it to grow significantly at all six energies (Fig. 9-left).

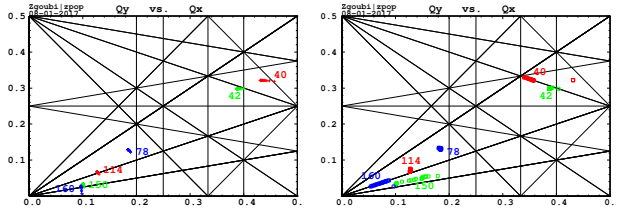

Figure 10: Spreading of Q_x, Q_y tunes under the effect of horizontal (left) and vertical (right) anharmonicities, up to maximum stable horizontal (left) and vertical (right) amplitude. Resonance lines $mQ_x + nQ_y$ =integer are for upright multipoles, up to $|m| + |n| = 5$. For each energy a few tune values are plotted, corresponding to particles launched with initial horizontal (vertical) invariants evenly distributed from paraxial to maximum amplitude.

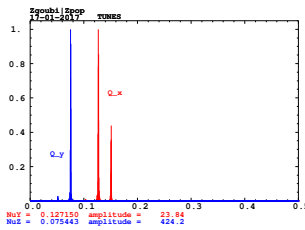

Figure 11: Non-linear motion spectrum at 114 MeV, case of maximum vertical amplitude. Red is horizontal motion, blue is vertical.

⋄ The effect of anharmonicities (*i.e.*, horizontal $dQ_x/d\epsilon_x$, $dQ_x/d\epsilon_y$, and vertical $dQ_y/d\epsilon_x$, $dQ_y/d\epsilon_y$) are represented in the tune diagrams in Fig. 10, via amplitude detuning for about 20 initial invariant values (for each one of the 6 energies considered) ranging evenly from paraxial up to maximum stable amplitude (as shown in Figs. 8 and 9). Tunes are computed by discrete Fourier transform, from 400-cell tracking. The two figures show respectively the case of large amplitude horizontal motion (that shown in Fig. 8) and large amplitude vertical motion (Fig. 9).

COMMENTS

Causes for non linear large amplitude motion and coupling have been addressed. The cell discussed was an intermediate stage in CBETA lattice design process, some of the drawbacks illustrated here have been overcome as part of that iterative process.

Note that this type of studies substantiates the need for a new class of lattice design programs, a leap in paradigm, namely, an innovative, interdisciplinary unified accelerator magnet/lattice design software tool, unifying a magnetostatics and a ray-tracing code in a common software environment, to allow magnet design constraints to be taken directly amongst beam dynamics properties, rather than solely from field properties, following a recent LDRD proposal at BNL [10].

ISBN 978-3-95450-182-3

REFERENCES

[1] D. Trbojevic, "CBETA: Cornell University Brookhaven National Laboratory ERL Test Accelerator", presented at IPAC'17, paper TUOCB3, this conference.

[2] N. Tsoupas et al., "The beam optics of the FFAG cell of the CBETA ERL accelerator", presented at IPAC'17, paper MOPIK122, this conference.

[3] F.T. Cole, "O Camelot! A Memoir of the Mura Years", April 1 1994, Secs. 6.7, 6.8.

[4] And including an FFAG beam line, see for instance : J.B. Lagrange et al., "Straight scaling FFAG beam line", NIM A, vol. 691, pp. 55-63, 2012.

[5] S. Machida et al., "Acceleration in the linear non-scaling fixed-field alternating-gradient accelerator EMMA", Nature Physics, vol. 8, pp. 243-247, 2012.

[6] https://sourceforge.net/projects/zgoubi/

[7] https://sourceforge.net/projects/pyzgoubi/

[8] S. Tygier, "PyZgoubi simulations of CBETA lattice", presented at IPAC17, Copenhagen, Denmark, May 2017, paper THPAB058, this conference.

[9] https://sourceforge.net/projects/zgoubi/

[10] F. Méot, O. Chubar, N. D'Imperio et al., "An innovative accelerator magnet/lattice design software tool", LDRD proposal, BNL, 2016.

ISBN 978-3-95450-182-3